Polymer Journal (2019) 51:173–182
https://doi.org/10.1038/s41428-018-0136-5

ORIGINAL ARTICLE

A study on the isothermal crystallization of poly(3-methylbutene-1)

Mizuki Kishimoto[1,2] · Kazuki Mita[1] · Junhyeok Jang[2] · Nobuaki Takahashi[2] · Hiroki Ogawa[2,3] · Koji Nishida[4] · Toshiji Kanaya[5] · Mikihito Takenaka[2,3]

Received: 20 August 2018 / Revised: 12 September 2018 / Accepted: 19 September 2018 / Published online: 2 November 2018

Abstract

Poly(3-methylbutene-1) (P3MB1) is a polyolefin with a high melting temperature T_m (≈ 305 °C). We investigated the structural evolution of P3MB1 during isothermal crystallization from the melt by synchrotron radiation X-ray scattering and polarizing optical microscopy. At crystallization temperatures (T_c) of 297 and 290 °C or shallow quench conditions ($\Delta T = T_m^0 - T_c = 26$ and 33 °C), needle-like crystals comprising lamellae were formed and flowed during their growth in the molten portion. To clarify the origin of the wide temperature region of the needle-like crystals in P3MB1, we estimated the critical lamellar width λ^*, which is a parameter characterizing the suppression of lamellar branching, of P3MB1 and polyethylene (PE). The λ^* of P3MB1 was larger than that of PE at the same ΔT, owing to the low viscosity of P3MB1. However, the range of λ^* in the temperature region of the needle-like crystals of P3MB1 was $0.41 < \lambda^* < 7.4$ μm; PE formed spherulites in this range. Thus, suppression is not only the origin of the needle-like crystals in P3MB1, but may also be responsible for the flow of the needle-like crystals in melts.

Introduction

Polyolefins such as polyethylene (PE) or polypropylene (PP) are important industrial materials owing to their excellent mechanical properties. One of the most important parameters of polyolefins is their melting temperature (T_m), which depends on their monomer structures. For example, the melting temperatures of PE and isotactic polypropylene (iPP) are approximately 120 °C and 160 °C, respectively; further, polyolefins show relatively poor heat resistance. Though isotactic poly(4-methylpentene-1) (P4MP1) has a high T_m (≈240 °C [1–3]) and shows relatively high heat resistance among commercially available polyolefins, polyolefins with higher heat resistance are required. Isotactic poly(3-methylbutene-1) (P3MB1) has a higher T_m (≈305 °C [4, 5]) than P4MP1 and is thus expected to be a new polymer material with high heat resistance. The chemical structure of P3MB1 is shown in Fig. 1c. However, P3MB1 is very brittle, and for practical use, its mechanical properties need to be improved by controlling the morphologies. Hence, it is very important to understand the formation process of the crystal structure of P3MB1. There are no studies on the isothermal crystallization of P3MB1, although there are studies regarding the crystal lattice [6–8] or the softening point [4, 5].

In this study, the changes in morphologies of P3MB1 during isothermal crystallization were investigated and discussed in conjunction with the measured thermodynamic parameters, such as the enthalpy of fusion, thickness, and surface free energy of lamellae, to understand the effect of the high T_m of P3MB1 on the crystallization dynamics.

Electronic supplementary material The online version of this article (https://doi.org/10.1038/s41428-018-0136-5) contains supplementary material, which is available to authorized users.

✉ Mizuki Kishimoto
Mizuki.Kishimoto@mitsuichemicals.com

[1] Process Technology Laboratory, Mitsui Chemicals, Inc., 580-32 Nagaura, Sodegaura, Chiba 299-0265, Japan

[2] Institute for Chemical Research, Kyoto University, Gokasho, Uji, Kyoto 611-0011, Japan

[3] Structural Materials Science Laboratory, SPring-8 Center, RIKEN Harima Institute Research, 1-1-1, Kouto, Sayo-cho, Sayo-gun, Hyogo 679-5148, Japan

[4] Department of Polymer Chemistry, Graduate School of Engineering, Kyoto University, Katsura, Nishikyo-ku, Kyoto 615-8510, Japan

[5] Material and Life Science Division, J-PARC, Institute of Material Structure Science, High Energy Accelerator Research Organization (KEK), Tokai-mura, Naka-gun, Ibaraki 319-1195, Japan

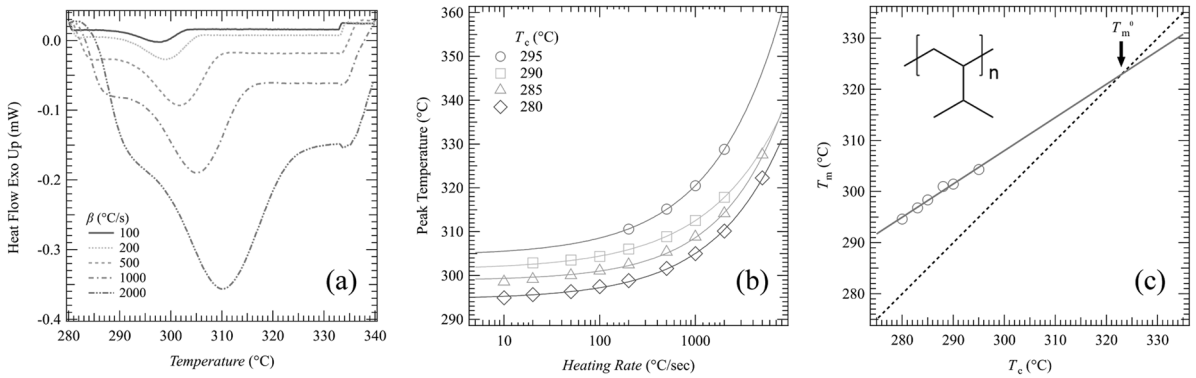

Fig. 1 **a** Melting behaviors of P3MB1 after isothermal crystallization at $T_c = 280$ °C measured by FSC. **b** β dependence of melting peak temperatures for P3MB1 crystallized at various T_c. The solid lines are the fitting curves expressed by Equation 1. **c** Hoffman-Weeks plots for P3MB1. $T_m^0 = 322.9$ °C

Since crystalline polymers form hierarchical structures over a wide spatial scale, it is necessary to employ various techniques to observe the hierarchical structures. For in situ observations over a wide spatial scale from 0.1 nm to several μm, optical microscopy (OM), small-angle X-ray scattering (SAXS), and wide-angle X-ray scattering (WAXS) measurements using synchrotron radiation were conducted. Fast scanning calorimetry (FSC) and pressure-volume-temperature (PVT) measurements were also conducted to evaluate the thermodynamic parameters of P3MB1.

Experimental procedure

P3MB1 powder was polymerized with conventional Ziegler-Natta catalysts. The P3MB1 powder was vacuum-pressed above T_m and quenched by cold pressing at room temperature, to obtain a film specimen of thickness 0.5 mm. We performed differential scanning calorimetry (DSC) measurements at a heating rate of 10 °C/min, and determined the T_m and the glass transition temperature (T_g) of P3MB1 to be 304 °C and 51 °C, respectively (Supplementary Material 1), which agree with the values reported previously [5, 9].

FSC measurements were performed with a Flash DSC (METTLER TOREDO) system. A 10 μm-thin film was cut out from the P3MB1 film specimen. The film was placed on a chip sensor and pre-melted at 340 °C for 1 s to ensure good adhesion to the sensor. Measurements were carried out as follows: First, the sample was held at 340 °C for 0.1 s, and quenched to the pre-set crystallization temperature (T_c) at a cooling rate of 4000 °C/s. After isothermal crystallization for 1 min, the sample was heated at the pre-set rate and the heat flow was recorded. T_c was set to a range of 220 to 295 °C, and the heating rate (β) was set to a range of 10 to 5000 °C/s.

The isothermal crystallization dynamics of P3MB1 was investigated at various T_c (297, 290 and 275 °C) after being quenched from the melt at T_i (348 °C). BX50 (Olympus) was used for OM. A piece of the film specimen was pressed to a thickness of 50 μm and sandwiched between two cover glasses to obtain a sample for the OM observations. Quench was attained as follows: First, the sample was set on the heater stage at T_i (heater stage I). After maintaining the sample for 5 min at T_i to erase the thermal history, it was slid from heater stage I to another heater stage at T_c (heater stage II). Subsequently, isothermal crystallization was observed. When the transfer was completed, the time (t) was set to zero.

Simultaneous synchrotron radiation SAXS and WAXS measurements were carried out under the same crystallization conditions as for the OM observation using the beamline BL03XU at SPring-8, Hyogo, Japan [10]. The wavelength of the incident X-rays was 0.1 nm. For the SAXS and WAXS measurements at $T_c = 297$ °C, a charge-coupled device camera with an image intensifier and a flat panel detector were used as detectors, the sample-to-detector distances were 2461 and 64 mm, and the exposure times were 100 and 330 ms, respectively; the scattering images were acquired every second. For the SAXS and WAXS measurements at $T_c = 290$ and 275 °C, Pilatus 1 M and a flat panel detector were used as detectors, the sample-to-detector distances were 2421 and 68 mm, and the exposure times were 670 and 670 ms, respectively; the scattering images were acquired every second. Quench was attained as follows: First, the specimens filled in sample cells with 12.5 μm-thick Kapton windows were set in a heater block at T_i (heater block I). After maintaining the samples for 5 min at T_i, the cell was transferred to another heater block (heater block II) set to T_c. When the transfer was completed, t was set to zero, as in the OM observations.

In addition, to calculate the enthalpy of fusion, another WAXS measurement was performed. The P3MB1 film was

placed in the abovementioned sample cell for the X-ray scattering experiment, and the WAXS measurements were performed in the range of 200–280 °C with NANO-Viewer (RIGAKU) and another heater block. PILATUS 10 K was used as a detector. The wavelength of the incident X-rays was 0.154 nm. The sample-to-detector distance was 91 mm, and the exposure time was 20 min.

The zero-shear viscosity (η) at 310 °C was measured by a rheometer, ARES (TA Instruments). The strain was 5% and the angular frequency was 0.1 to 500 rad/s.

PVT measurements were performed with the GNOMIX apparatus. A few pieces of the P3MB1 film were vacuum-dried at 80 °C for 4 h and then sealed in the sample cell. The change in the specific volume during isobaric heating was recorded. The pressure was set to a range of 20 to 100 MPa, and the heating rate was 4 °C/min. The temperature dependence of the specific volume at 0 MPa was calculated from the results of the isothermal measurement in the range of 10–30 MPa.

Results and discussion

Determination of T_m^0 of P3MB1 by FSC measurement

We estimated the equilibrium melting temperature (T_m^0) by using the Hoffman-Weeks (H-W) plot [11] with the FSC measurements [12, 13]. In the H-W plots, the intersection between $T_m = T_c$ and the linear line extrapolated from the plots of $T_m(T_c)$ vs T_c corresponds to T_m^0, where $T_m(T_c)$ is the melting temperature of the crystals crystalized at T_c. We can estimate $T_m(T_c)$ by measuring the β dependence of T_m during quick melting processes from the crystals crystalized at T_c, with the FSC measurements. It should be noted that slow cooling induces crystallization during the cooling processes with conventional DSC measurements; therefore, we cannot obtain the crystals crystalized at T_c and estimate $T_m(T_c)$ correctly with slow cooling. Fig. 1a shows the β dependence of the heat flow during heating processes in the P3MB1 samples crystalized at $T_c = 280$ °C. We can observe the peaks corresponding to T_m in each curve. As β decreases, the peak temperature T_p shifts to a lower temperature. We also measured the β dependence of the heat flow for the P3MB1 samples crystalized at $T_c = 283$–295 °C. At $T_c <$ 280 °C, the crystallization occurred during quenching; hence, $T_m(T_c)$ could not be evaluated accurately. Figure 1b shows the β dependence of $T_p(T_c)$ for various T_c. According to Toda et al. [14]., the β dependence of $T_p(T_c)$ for T_c is expressed by

$$T_p(T_c) = T_m(T_c) + A\beta^z \quad (1)$$

where A and z are constants. The solid lines are the fitting results with Eq. 1, showing that Eq. 1 can express the experimental results and we can estimate $T_m(T_c)$ for 280–295 °C. Figure 1c shows the H-W plot or $T_m(T_c)$ as a function of T_c. The plot shows a linear relationship, and T_m^0 ($= 322.9$ °C) is obtained from the intersection between the line of $T_m = T_c$ and the linear line extrapolated from the plot of $T_m(T_c)$ vs. T_c.

OM observation during isothermal crystallization

The OM images at each T_c are shown in Fig. 2. The OM images at $T_c = 275$ °C were observed under the crossed Nicols condition. In contrast, we observed the OM images under the parallel Nicols conditions at $T_c = 290$ and 297 °C, because we could not obtain enough contrast under the crossed Nicols condition. As shown in Fig. 2a, needle-like crystals developed during the isothermal crystallization at $T_c = 297$ °C. At $t = 580$ s, the longitudinal size of the crystals reached 100 μm. This morphology is quite different from that of the spherulites commonly observed in PE. In addition, the needle-like crystals flow in the melts, as shown in a video (Supplementary Material 2).

At $T_c = 290$ °C, the needle-like crystals and axialites coexisted (Fig. 2b). The change in morphology was not observed after $t = 40$ s. The needle-like crystals flow while the axialites appear not to flow in the melts. We could not observe the needle-like crystals and the axialites clearly under the crossed Nicols condition. These crystals are considered thinner than spherulites, and hence cannot make sufficient retardation.

At $T_c = 275$ °C, isotropic crystals grew immediately after quenching and collided with each other, following which the growth stopped (Fig. 2c). We could not distinguish whether these crystals were in the form of spherulites or axialites. Kirshenbaum et al. [5] observed spherulites of P3MB1 more clearly by slow cooling. The OM observations at $T_c = 275$–297 °C indicate that as T_c increased, the number of lamellar branches decreased, and the spherulites changed to needle-like crystals via axialites.

SAXS and WAXS measurements during isothermal crystallization

Figure 3 shows the scattering patterns obtained by time-resolved SAXS and WAXS measurements at each T_c, and Fig. 4 shows the circular averaged profiles corresponding to the pattern. Here, q is the magnitude of the scattering vector defined by $q = (4\pi/\lambda)\sin(\theta/2)$, where λ and θ are the wavelength of the incident X-rays and the scattering angles, respectively. As seen in the SAXS patterns at 297 °C (left side of Fig. 3a), peaks from the long period of the stacked

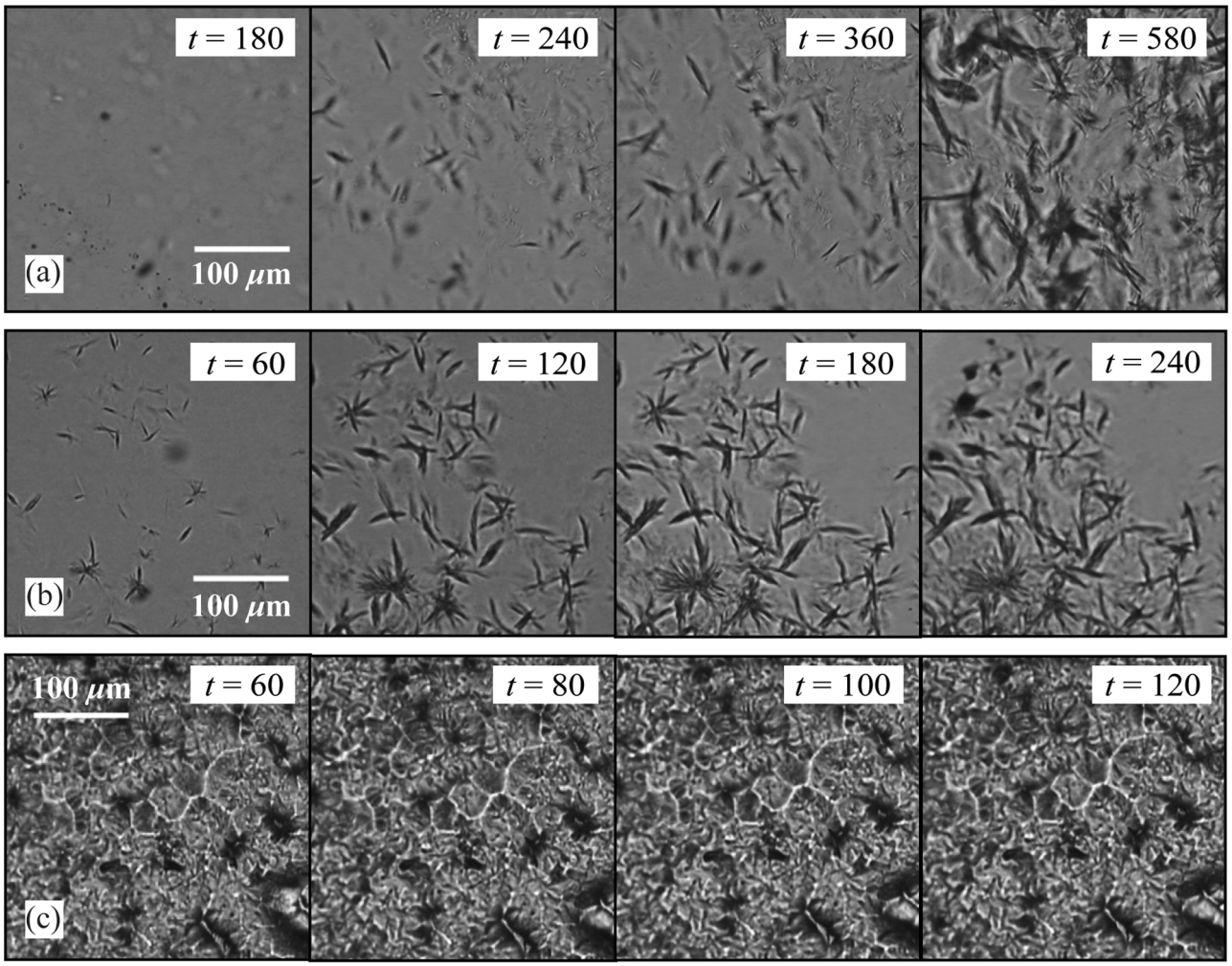

Fig. 2 Representative OM images at $T_c =$ **a** 297 °C, **b** 290 °C, and **c** 275 °C. **c** was obtained under the crossed Nicols condition

lamellae were observed, except at $t = 240$ s, and the patterns possessed anisotropy even though the crystallization occurred in the static field. In the WAXS patterns, anisotropic patterns with multiple diffracted spots in the azimuthal direction were observed (right side of Fig. 3a). As seen in the representative profiles, peaks from the long period were observed up to the second order in SAXS (Fig. 4a), whereas in WAXS, the diffraction peaks attributed to monoclinic crystals were observed, and no other crystal systems were obtained (Fig. 4b). To clarify the change in lamellar structures, we fitted the series of SAXS profiles around the primary peak with Eq. 2:

$$I(q) = Bq^{-n} + I_{\mathrm{lp}}\exp\left\{-\frac{(q - x_{\mathrm{lp}})^2}{w_{\mathrm{lp}}}\right\} \tag{2}$$

Equation 2 is a linear combination of the power law and the Gaussian function, where I_{lp}, x_{lp}, and w_{lp} are the peak intensity, position and width, respectively. We also fitted the series of WAXS profiles at $q < 8\,\mathrm{nm}^{-1}$ with Eq. 3. Equation 3 is a linear combination of three Gaussian functions and a constant I_{base}; the first term is the amorphous contribution, whereas the second and third terms are the contributions from the lattice planes corresponding to the subscripts.

$$I(q) = I_{\mathrm{am}}\exp\left\{-\frac{(q - x_{\mathrm{am}})^2}{w_{\mathrm{am}}}\right\} + I_{100}\exp\left\{-\frac{(q - x_{100})^2}{w_{100}}\right\} + I_{010,1\bar{1}0}\exp\left\{-\frac{\left(q - x_{010,1\bar{1}0}\right)^2}{w_{010,1\bar{1}0}}\right\} + I_{\mathrm{base}} \tag{3}$$

The lattice spacings of (010) and $(1\bar{1}0)$ are mutually too close to distinguish on the profiles. Figure 4c shows the time evolutions of the peak intensities, I_{lp} and I_{100},

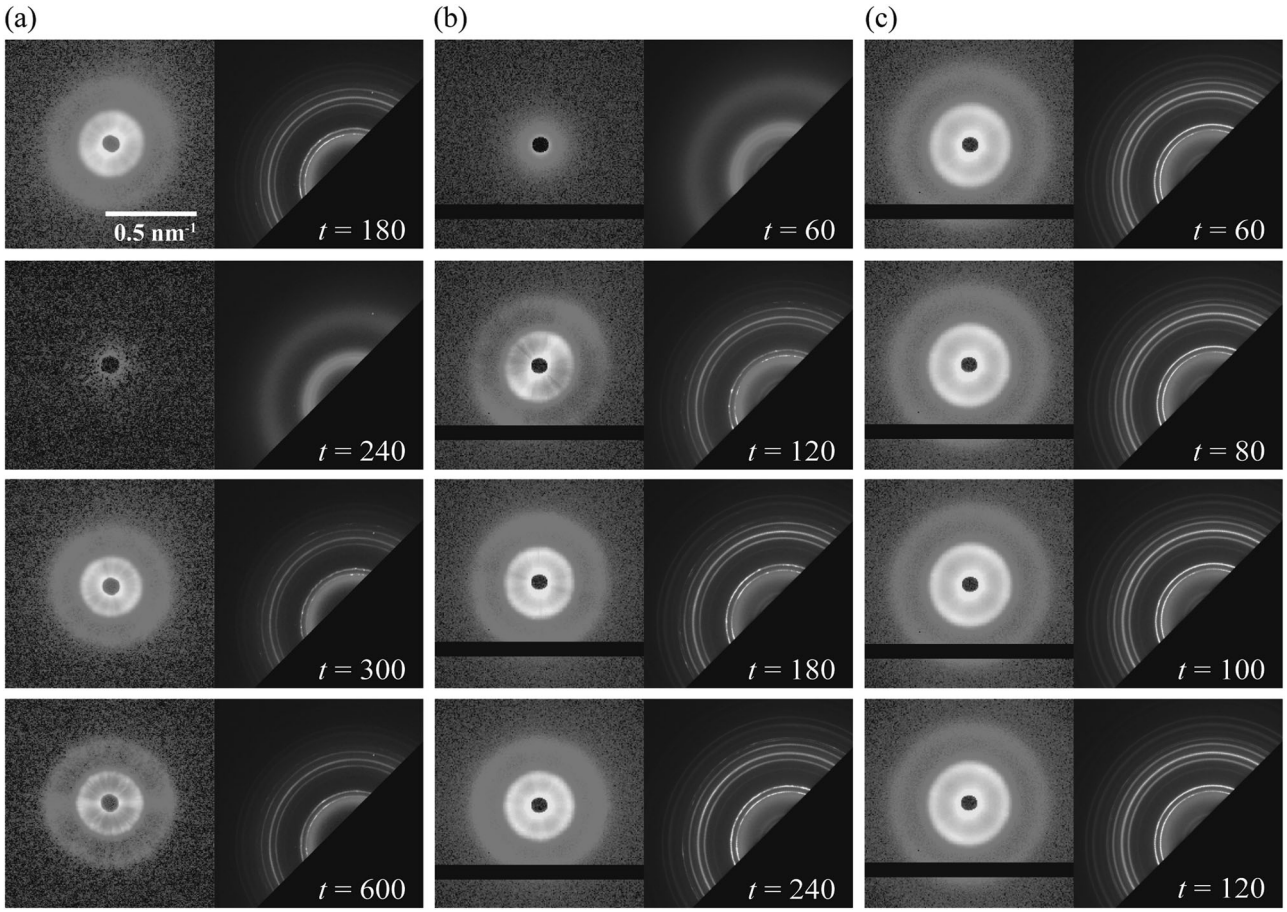

Fig. 3 Representative SAXS and WAXS patterns at $T_c =$ **a** 297 °C, **b** 290 °C, and **c** 275 °C. The left side of each set shows the SAXS patterns. The black lines at the bottom of the SAXS patterns of **b** and **c** represent the gap between the detector modules

which repeatedly increase and decrease irregularly with time. At $t = 240$ s, no signals from the crystals were detected in either SAXS or WAXS. This fluctuation in the peak intensities suggests that the amount of the crystalline region in the irradiated area (120 × 80 μm) of the incident X-ray beam changes irregularly with time due to the flow of the crystalline structures in the melt. This also indicates that we cannot discuss the crystallization kinetics of P3MB1 with the time-resolved X-ray scattering data. A similar tendency can be observed at $T_c =$ 290 °C. The anisotropic SAXS and WAXS patterns can be seen at $T_c =$ 290 °C (Fig. 3b). The time evolutions of the peak intensities (Fig. 4f) increase in the SAXS and WAXS profiles with fluctuations. In the case of $T_c = 275$ °C, the isotropic SAXS and WAXS patterns were well developed even at $t = 60$ s, and a slight increase in the intensities was observed thereafter (Fig. 3c). The time evolutions of the peak intensities also show that the changes in the intensities after $t =$ 60 s were very small.

Furthermore, in the changes in the SAXS and WAXS profiles with time at $T_c = 297$ °C, since the moments of the appearance/disappearance of the long periods and the diffraction peaks were synchronized, a lamella stack was found in the needle-like crystals. The needle-like crystals reported thus far have been limited to single crystals, and those with stacked lamellae have not yet been discovered, to the best of our knowledge. In polyolefins, PE and P4MP1 form extended-chain single crystals under high pressures [15, 16]. Such single crystals consist of hexagonal crystal lattices, with thicknesses on the order of micrometers. Moreover, PP forms giant single crystals via the meso phase [17]. As mentioned above, hexagonal crystals of P3MB1 were not observed in our WAXS measurements. If the needle-like crystals in P3MB1 were single crystals, then the lamellae composed of monoclinic crystal lattices would have a thickness on the order of micrometers. In that case, $T_m \simeq T_m{}^0$ and especially at $T_c >$ 290 °C, two melting peaks should be obtained in the thermal analysis, since the single crystals coexist with the lamellae with a thickness of tens of nanometers. However, in the series of FSC measurements mentioned above, the melting peak was always unimodal at $T_c = 280$–295 °C,

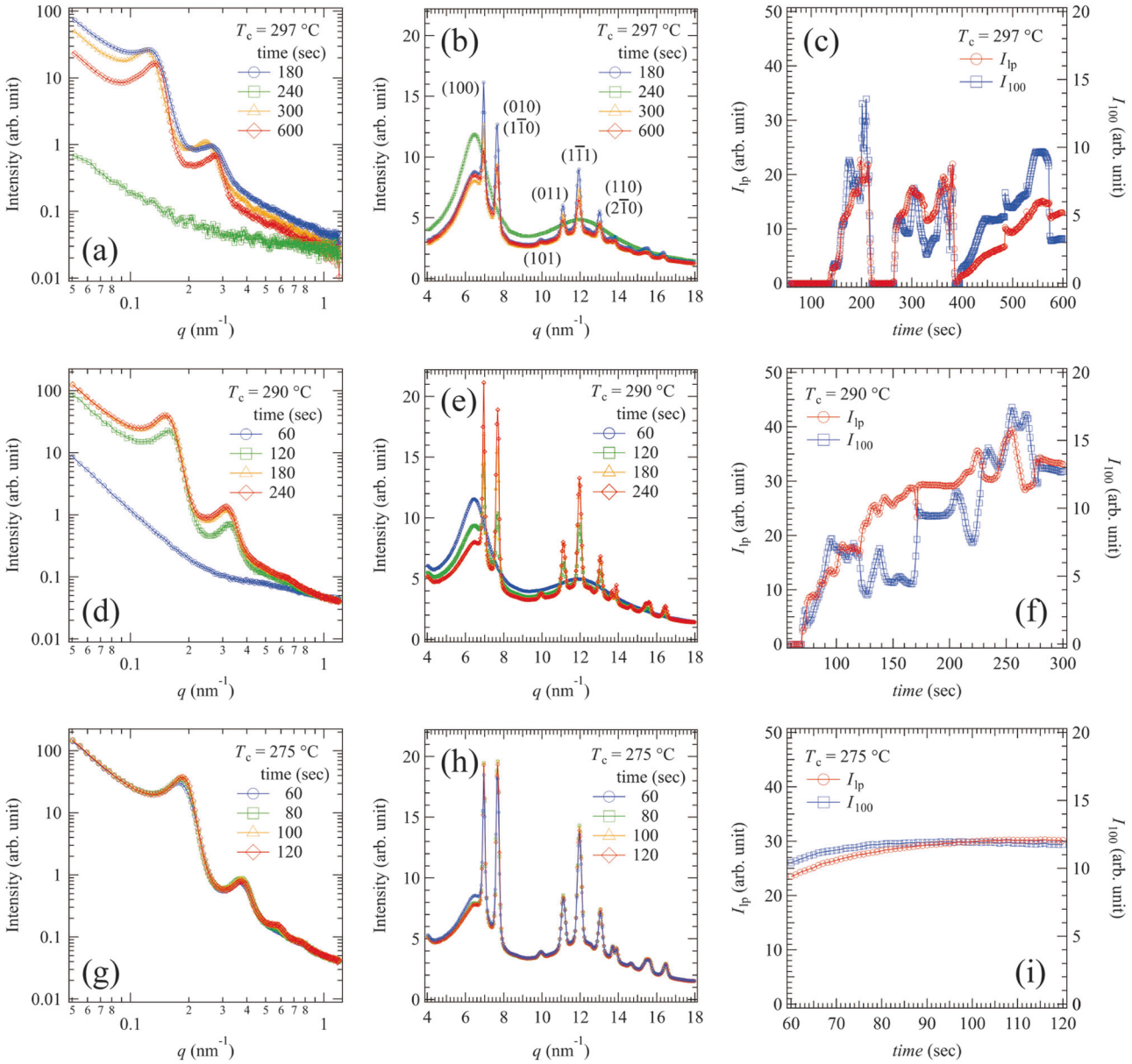

Fig. 4 Representative SAXS profiles at T_c = **a** 297 °C, **d** 290 °C, and **g** 275 °C; WAXS profiles at T_c = **b** 297 °C, **e** 290 °C, and **h** 275 °C; time evolutions of the peak intensities I_{lp} and I_{100} defined in Equations 2 and 3 at T_c = **c** 297 °C, **f** 290 °C, and **i** 275 °C

and T_m continued to increase as T_c increased, as shown in the H-W plots (Fig. 1c). This indicates that the needle-like crystals of P3MB1 are not single crystals but are composed of stacked lamellae, which are nanometer-thick folded chain crystals.

Growth of needle-like crystals in P3MB1

As shown in the previous section, needle-like crystals are formed in P3MB1 in the wide ΔT region. It was reported that the number of lamellar branches decreases as T_c increases in PE and isotactic poly(butene-1) (PB1) [18, 19]. Granasy et al. [20] have reported a morphological transition from spherulites to needle-like crystals with a decrease in supersaturation by computer simulation. In addition, in the high T_c region, PE is reported to often form axialites with a regime transition (II → I) [21, 22]. Regime I and II represent the single- and multi-nucleation growth, respectively. However, the region of the axialites of PE is much narrower than that of P3MB1.

We examined why P3MB1 has less lamellar branches than PE. One reason may be the morphological instability caused by the gradient of the chemical potential spontaneously generated at the growth front. Toda et al. [18]

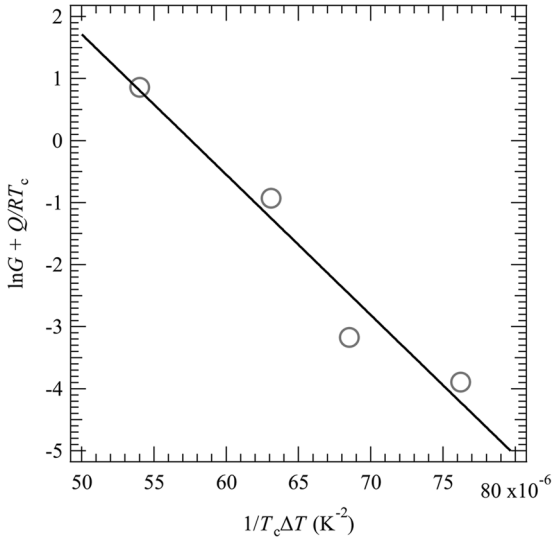

Fig. 5 Plots of $\ln G + Q/RT_c$ vs. $1/T_c\Delta T$. $G_0 = 4.56 \times 10^5$ cm/s and $K = 2.26 \times 10^5$ K^2

attributed this gradient to the pressure field, that is, the difference in the densities of the crystal and the melt [19]. In their model, decreasing branches and increasing lamellar widths were synonymous. The critical lamellar width λ^* under a pressure field can be expressed as

$$\lambda^* = 2\pi b_f \frac{v_c}{\Delta v}\left(\frac{\sigma}{12G\eta}\right)^{\frac{1}{2}} \tag{4}$$

where b_f, v_c, Δv, σ, G, and η are the thickness of the shear flow induced by the gradient field, specific volume of the crystal, difference between the specific volume of the crystal and the melt, surface free energy of the growth front, crystal growth rate and viscosity at T_c, respectively. It is known that b_f is as large as the bundle of lamellae in the melt; hence, in this study, b_f is equivalent to the lamella thickness (d). In the following part, we shall describe the estimation of λ^*. To estimate the values of λ^*, we need b_f, v_c, Δv, η, G, and σ. Several G values were determined from the microscope observations at $T_c = 290$–300 °C. The time evolutions of the size in the longitudinal direction of several needle-like crystals were investigated. Subsequently, considering their anisotropies, the largest G value in each T_c was adopted. Finally, the value was halved. As stated above, axialites are commonly observed in regime I. Hence, we assumed that the P3MB1 crystals grow in regime I, at least for $T_c > 290$ °C. According to the surface nucleation theory of Lauritzen and Hoffman, G is expressed as [22]

$$G = G_0 \exp\left(\frac{-Q}{RT_c}\right)\exp\left(\frac{-K}{T_c\Delta T}\right) \tag{5}$$

Particularly in regime I,

$$K = \frac{4b_0\sigma\sigma_e T_m^0}{k\Delta H} \tag{6}$$

where G_0, Q, R, b_0, σ_e, k, and ΔH are the preexponential factor, activation energy of the chain motion in the melt, gas constant, thickness of the molecular stem, fold surface free energy, Boltzmann constant and enthalpy of fusion, respectively. They are all constants independent of the temperature in this study ($\Delta T = T_m{}^0 - T_c$). Q of P3MB1 was calculated from the viscoelasticity data of Takayanagi [23]. $Q = \ln a_T R T_1 T_2/(T_2 - T_1) = 40$ kJ/mol. Here, a_T is the shift factor and $\ln a_T = 2.63$, $T_1 = 363$ K and $T_2 = 453$ K. Equation 5 was transformed as $\ln G + Q/RT_c = \ln G_0 - K/T_c\Delta T$, and the $\ln G + Q/RT_c$ vs. $1/T_c\Delta T$ plot was obtained (Fig. 5). Assuming that $T_c =$ 290–300 °C is the range of regime I and fitted to a linear line, G_0 and K were obtained from the ordinate intercept and the slope, respectively. All parameters for Eq. 5 are shown in Table 1. For comparison, those of PE ($M_w =$ 74,400, $M_w/M_n = 1.12$) reported by Armistead and Hoffman are also listed.

To evaluate σ in Eq. 6, the following analyses were conducted. First, ΔH was calculated from the Clausius-Clapeyron equation [2], expressed as

$$\Delta H = T_m(V_l - V_c)/\frac{dT_m}{dP} \tag{7}$$

here, V_l and V_c are the atmospheric pressure volumes of the melt and the crystal at T_m, respectively. dT_m/dP is the dependence of T_m on pressure. Selected isobars in the PVT relationship of P3MB1 are shown in Fig. 6. The intersection points of the black solid lines correspond to T_m. $V_l =$ 1.439 cm^3/g was obtained by fitting the volume at 0 MPa and $T > T_m$ to a quadratic function. Figure 7 shows the pressure dependence of T_m of P3MB1. The solid line is the fitting curve expressed by a third-order polynomial. By differentiating it, we obtained $dT_m/dP = 0.844$ °C/MPa. The results of the WAXS measurements to evaluate V_c are provided in Supplementary Material 3. Finally, $\Delta H = 113$ J/cm^3 was calculated. All parameters for Eq. 7 are shown in Table 2.

Next, σ_e was obtained using the Gibbs-Thomson equation expressed by [11]

$$T_m = T_m^0\left(1 - \frac{2\sigma_e}{\Delta H d}\right) \tag{8}$$

d was calculated from the SAXS profile at $T_c = 290$ °C and $t = 300$ s (Supplementary Material 4) [24]. The results of FSC were used for T_m. Corradini et al. reported a P3MB1 monoclinic unit cell with $a = 9.55$ Å, $b = 8.54$ Å, $c =$ 6.84 Å, $\gamma = 116.30°$ [6]. From these values, the lattice

Table 1 Parameters for P3MB1 and PE in Equation 5

	P3MB1	PE ($M_w = 74{,}400$, $M_w/M_n = 1.12$)
T_m^0 (K, °C)	596.1, 322.9	417.9, 144.7 (ref. 29)
Q (kJ/mol)	40.0	24.0 (ref. 30)
G_0 for regime I, II, III (cm/s)	4.56×10^5 (assume regime I)	1.4×10^{10}, 1.02×10^3, 1.65×10^7 (ref. 22)
K for regime I, II, III (K^2)	2.26×10^5 (assume regime I)	1.98×10^5, 0.940×10^5, 1.85×10^5 (ref. 22)

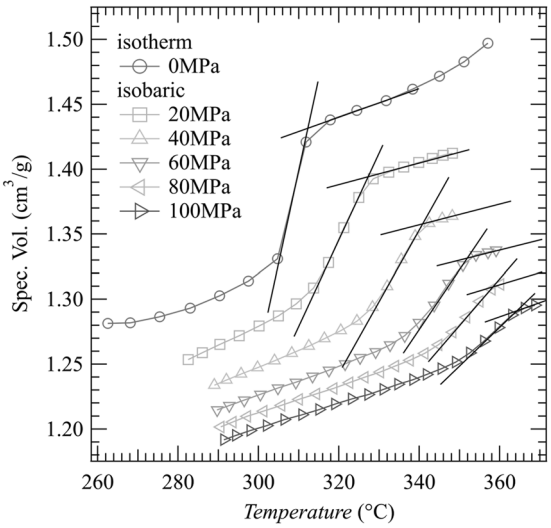

Fig. 6 Selected isobars in the PVT relationship of P3MB1. The 0 MPa volume was extrapolated from the isotherm measurements at 10–30 MPa. The intersection points of the black solid lines correspond to T_m

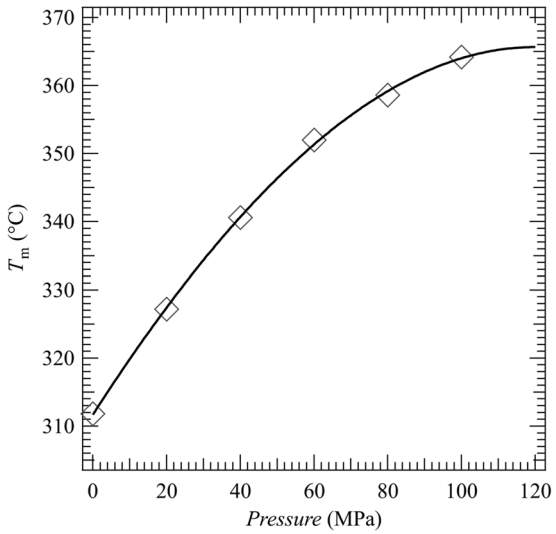

Fig. 7 Pressure dependence of T_m of P3MB1. The solid line is the fitting curve expressed by a third-order polynomial

Table 2 Parameters for Equation 7

T_m	V_l	V_c	dT_m/dP	ΔH
585 K 312 °C	1.439 cm^3/g	1.103 cm^3/g	0.844 °C/MPa	113 J/cm^3 124 J/g

spacings of the (100), (010), and (110) planes were calculated to be 8.56, 7.66, and 7.63 Å, respectively. Here, we assumed the value of the (110) plane as b_0. Finally, σ was obtained from Eq. 6. All parameters for Eq. 6 are shown in Table 3. The σ_e and σ values of P3MB1 are both smaller than those of PE.

The ΔT dependence of λ^* was calculated by Eq. 4 and is shown in Fig. 8 for each polymer. Note that the curve of P3MB1 was calculated by assuming regime I for $T_c =$ 290–300 °C. The η of P3MB1 at 310 °C was 51.4 Pa·s. Hence, the temperature dependence of η was obtained by the Andrade equation [25], $\eta = \eta_0 \exp(Q/RT) = 1.3 \times 10^{-2} \exp(4.8 \times 10^2/T)$. Using the same way as Toda et al., we calculated the η of PE from the Vogel-Fulcher equation based on the results of Pearson et al. [26]. The d values of both polymers were evaluated by Eq. 8. The T_m of PE was obtained by considering the doubling of the lamellar thickness ($T_m = (T_c + T_m^0)/2$) [12]. The value of $v_c/\Delta v$ is 4.5 [27, 28].

Comparing at the same ΔT, P3MB1 has a larger λ^* than PE and forms axialites or needle-like crystals in the range where PE forms spherulites. All parameters for P3MB1 at $T_c = 297$ °C and PE at the same ΔT (26 °C) as for P3MB1 are shown in Table 4. The difference in η affects λ^* most strongly. Hence, one of the most significant factors for the suppression of branching in P3MB1 was the low η at T_c. Of course, the η of P3MB1 is higher than that of PE at the same temperature, due to its bulkier side group. However, P3MB1 has a very high T_m and often crystallizes with a low η that cannot be reached when PE crystallizes. In such a case, the characteristic morphology may be observed.

However, the range of λ^* in the temperature region where the needle-like crystals of P3MB1 were observed is $0.41 < \lambda^* < 7.4$ μm, and PE forms the spherulites in the same range of λ^*, indicating that suppression is not the only origin of the needle-like crystals in P3MB1. We believe that another reason may be the flow of the needle-like crystals in the melts. As observed in the OM images, the low viscosity induces the flow of the needle-like crystals. The flow may induce the local orientation of the polymer chains in the melts and the orientation might suppress the branching.

Table 3 Parameters for P3MB1 and PE in Equation 6

	P3MB1	PE ($M_w = 74{,}400$, $M_w/M_n = 1.12$)
ΔH (J/cm^3, J/g)	113, 124	280, 293 (ref. 31)
d (nm)	16.3 ($T_c = 290$ °C, $T_m = 301$ °C)	-
b_0 (Å)	7.63 ((110) plane spacing)	4.15 (ref. 31)
σ_e (J/cm^2)	3.29×10^{-6}	9.0×10^{-6} (ref. 31)
σ (J/cm^2)	5.87×10^{-7}	11.8×10^{-7} (ref. 31)

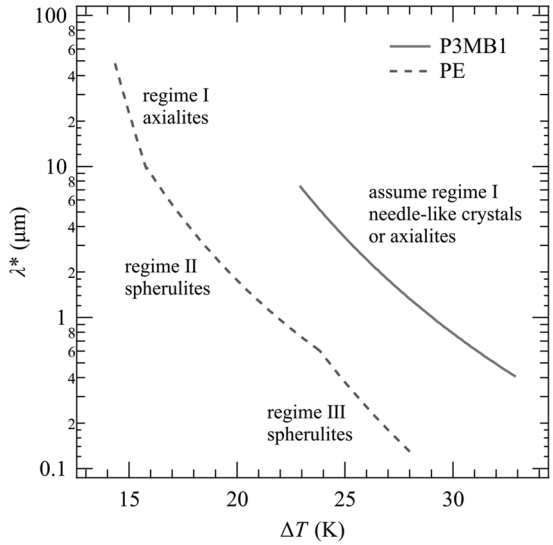

Fig. 8 ΔT dependence of λ^* of P3MB1 and PE ($M_w = 74{,}400$, $M_w/M_n = 1.12$) calculated by Equation 4

Table 4 Parameters for P3MB1 and PE in Equation 4 at $\Delta T = 26$ °C

	P3MB1	Calculated by
b_f (nm)	21 ($T_c = 297$ °C, $T_m = 306$ °C)	Equation 8, FSC, and SAXS data
$v_c/\Delta v$	3.2	WAXS and PVT data
G (cm/s)	1.8×10^{-5}	Equation 5 and Table 1
η (Pa·s)	62	Andrade equation, η at 310 °C and ref. 23
λ^* (μm)	2.8	Equation 4
PE ($M_w = 74{,}400$, $M_w/M_n = 1.12$)		Calculated by
b_f (nm)	21 ($T_c = 119$ °C, $T_m = 132$ °C)	Equation 8 and refs. 12, 22
$v_c/\Delta v$	4.5	ref. 27, 28
G (cm/s)	1.0×10^{-4}	ref. 22
η (Pa·s)	3.8×10^3	ref. 26
λ^* (μm)	0.30	Equation 4

Conclusion

We investigated the isothermal crystallization of P3MB1, a polyolefin with a high melting temperature, after the onset of quench from the molten state by OM observations and time-resolved SAXS and WAXS measurements. At $T_c = 297$ °C, the OM observations revealed that needle-like crystals were formed and moved in melt matrices. Anisotropic scattering patterns were observed in SAXS and WAXS at 297 °C, and the anisotropies and the scattering intensities changed irregularly with time. The irregular changes in scattered intensity are due to the flow of the needle-like crystals in and out of the irradiated area of the incident X-ray beam. This needle-like crystal is not a single crystal, but one composed of stacked lamellae.

As T_c increased, the morphological transition from spherulites to needle-like crystals was considered to occur via axialites. In other words, the needle-like crystals were considered axialites without lamellar branches. To elucidate the origin of the suppression of branching, we evaluated thermodynamic parameters such as ΔH, d, and σ, and calculated λ^* for P3MB1 and PE. λ^* for P3MB1 was larger than that for PE, suggesting that the suppression of branching is due to the low η at T_c. The low viscosity also induces the local orientation of the polymer chains in the melts, and this orientation might suppress branching.

Acknowledgements This work was partially supported by Photon and Quantum Basic Research Coordinated Development Program of MEXT. The SAXS and WAXS measurements in this study were conducted with the approval of SPring-8 (Grant Nos. 2013B7266, 2014A7217, 2014B7266, 2015B7267, 2016A7217, 2016B7266, and 2017A7215).

Compliance with ethical standards

Conflict of interest The authors declare that they have no conflict of interest.

References

1. Charlet G, Delmas G. Heat of fusion of poly(4-methylpentene-1). J Polym Sci Part B: Polym Phys. 1988;26:1111–25.
2. Zoller P, Starkweather HW, Jones GA. The heat of fusion of poly (4-methyl pentene-1). J Polym Sci Part B: Polym Phys. 1986;24:1451–8.
3. Mita K, Okumura H, Kimura K, Isaki T, Takenaka M, Kanaya T. Simultaneous small- and wide-angle X-ray scattering studies on the crystallization dynamics of poly(4-methylpentene-1) from melt. Polym J. 2012;45:79–86.

4. Quynn RG, Sprague BS. Physical structure and properties of 3-methylbutene-1 polymer and fiber. J Polym Sci Part A-2: Polym Phys. 1970;8:1971–85.
5. Kirshenbaum I, Feist WC, Isaacson RB. Properties of semi-crystalline polyolefins. IV. Crystallization phenomena in poly-3-methyl-1-butene. J Appl Polym Sci. 1965;9:3023–31.
6. Corradini P, Ganis P, Petraccone V. Crystal structure of isotactic poly(3 methyl butene-1). Eur Polym J. 1970;6:281–91.
7. Utsunomiya H, Kawasaki N, Niinomi M, Takayanagi M. Single crystals of isotactic poly-3-methyl-butene-1. J Polym Sci Part B: Polym Lett. 1967;5:907–10.
8. Jones AT, Aizlewood JM. Crystalline forms of polypentene-1. J Polym Sci Part B: Polym Lett. 1963;1:471–6.
9. Reding FP, Faucher JA, Whitman RD. Glass transitions in ethylene copolymers and vinyl homopolymers and copolymers. J Polym Sci. 1962;57:483–98.
10. Masunaga H, et al. Multipurpose soft-material SAXS/WAXS/GISAXS beamline at SPring-8. Polym J. 2011;43:471–7.
11. Hoffman JD, Weeks JJ. Rate of spherulitic crystallization with chain folds in polychlorotrifluoroethylene. J Chem Phys. 1962;37:1723–41.
12. Toda A, Taguchi K, Nozaki K, Konishi M. Melting behaviors of polyethylene crystals: An application of fast-scan DSC. Polym (Guildf). 2014;55:3186–94.
13. Furushima Y, Nakada M, Takahashi H, Ishikiriyama K. Study of melting and crystallization behavior of polyacrylonitrile using ultrafast differential scanning calorimetry. Polym (Guildf). 2014;55:3075–81.
14. Toda A, Androsch R, Schick C. Insights into polymer crystallization and melting from fast scanning chip calorimetry. Polym (Guildf). 2016;91:239–63.
15. Hikosaka M, Amano K, Rastogi S, Keller A. Lamellar thickening growth of an extended chain single crystal of polyethylene. 1. Pointers to a new crystallization mechanism of polymers. Macromolecules. 1997;30:2067–74.
16. Rastogi S, Höhne GWH, Keller A. Unusual pressure-induced phase behavior in crystalline poly(4-methylpentene-1): Calorimetric and spectroscopic results and further implications. Macromolecules. 1999;32:8897–909.
17. Asakawa H, Nishida K, Kanaya T, Tosaka M. Giant single crystal of isotactic polypropylene showing near-equilibrium melting temperature. Polym J. 2013;45:287–92.
18. Toda A, Okamura M, Taguchi K, Hikosaka M, Kajioka H. Branching and higher order structure in banded polyethylene spherulites. Macromolecules. 2008;41:2484–93.
19. Kajioka H, Hikosaka M, Taguchi K, Toda A. Branching and re-orientation of lamellar crystals in non-banded poly(butene-1) spherulites. Polym (Guildf). 2008;49:1685–92.
20. Gránásy L, Pusztai T, Tegze G, Warren JA, Douglas JF. Growth and form of spherulites. Phys Rev E. 2005;72:011605.
21. Hoffman JD, Frolen LJ, Ross GS, Lauritzen JI, Jr. On the growth rate of spherulites and axialites from the melt in polyethylene fractions: Regime I and regime II crystallization. J Res Nat Bur Stand. 1975;79A:671–99.
22. Armistead JP, Hoffman JD. Direct evidence of regimes I, II, and III in linear polyethylene fractions as revealed by spherulite growth rates. Macromolecules. 2002;35:3895–913.
23. Takayanagi M. Some structural factors in low temperature transitions of Polymers. Pure Appl Chem. 1970;23:151–82.
24. Strobl G. The physics of polymers. Berlin: Springer; 2007.
25. Andrade ENdCLVIII. A theory of the viscosity of liquids.—Part II. Lond Edinb Dub Philos Mag J Sci. 1934;17:698–732.
26. Pearson DS. Viscosity and self-diffusion coefficient of linear polyethylene. Macromolecules. 1987;20:1133–41.
27. Orwoll RA. Equation-of-state parameters for normal alkanes. Correlation with chain length. J Am Chem Soc. 1967;89:6814–22.
28. Coles EA, Holmes DR. Crystal lattice parameters and the thermal expansion of linear paraffin hydrocarbons, including polyethylenes. J Polym Sci. 1960;46:245–56.
29. Flory PJ, Vrij A. Melting points of linear-chain homologs. The normal paraffin hydrocarbons. J Am Chem Soc. 1963;85:3548–53.
30. Fletcher DP, Klein J. Temperature depemdence of the diffusion coefficient of entangled linear and star-branched polymers. J Polym Commun. 1985;26:2–4.
31. Hoffman JD, Miller RL. Kinetic of crystallization from the melt and chain folding in polyethylene fractions revisited: theory and experiment. Polym (Guildf). 1997;38:3151–212.